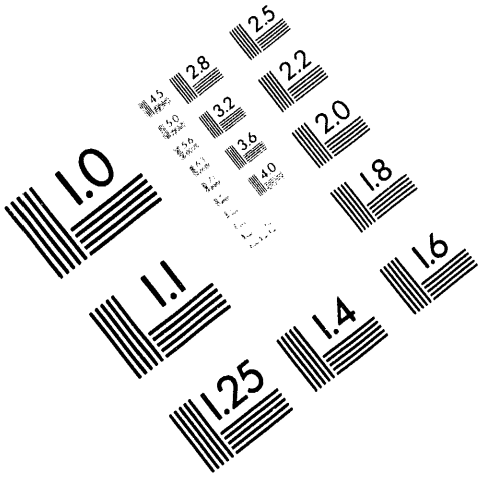

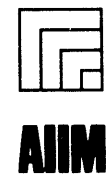

Association for Information and Image Management

1100 Wayne Avenue, Suite 1100
Silver Spring, Maryland 20910

301/587-8202

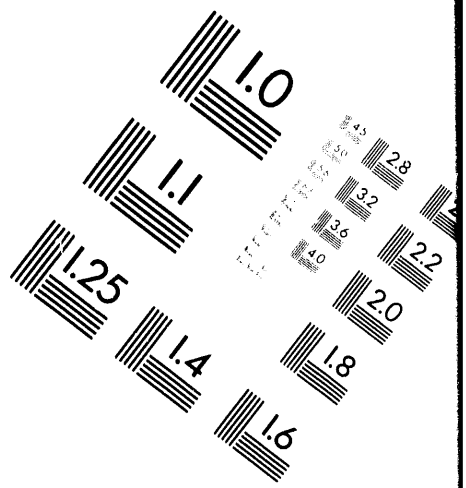

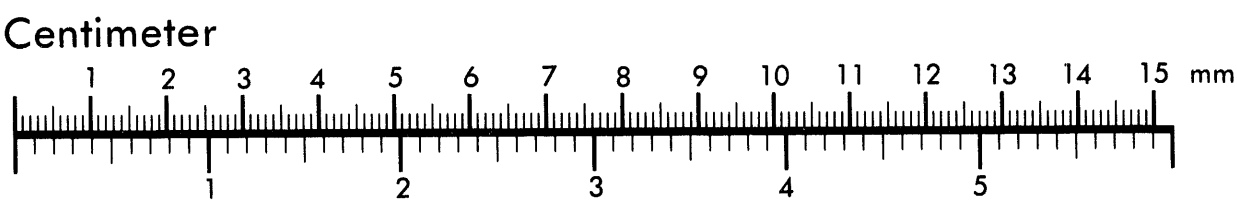

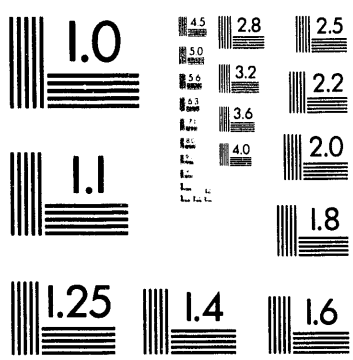

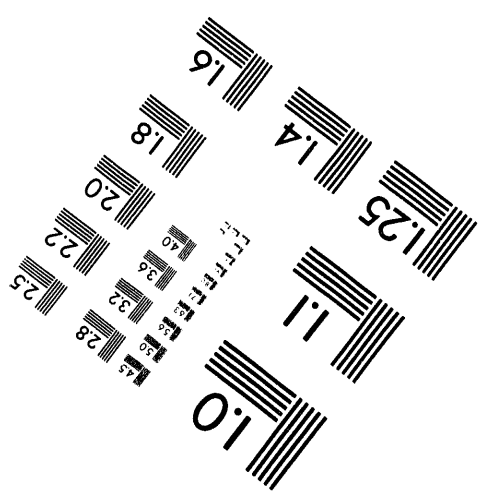

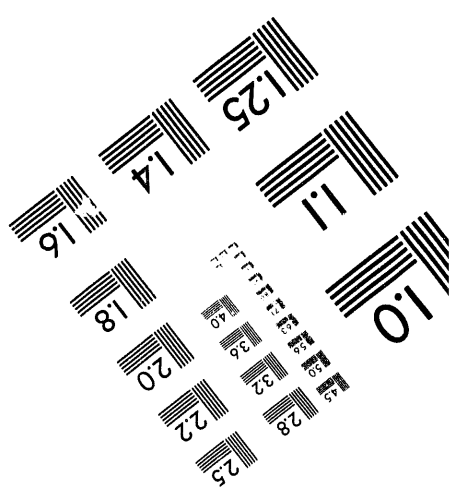

1 of 1

Conf-9410131--2
SAND94-0058C

Version of June 9, 1994 11:56 pm
SAND 94-0058C

Draft Version
HVIS 160F (1994 HVIS)

Dynamical Properties Measurements for Asteroid, Comet and Meteorite Material Applicable to Impact Modeling and Mitigation Calculations*

M. D. FURNISH and M. B. BOSLOUGH
Dept. 1433, MS 0821, Sandia National Laboratories, Albuquerque, NM 87185

G. T. GRAY III
MST-5, MS G730, Los Alamos National Laboratories, Los Alamos NM 87545

J. L. REMO
Quantametrics, Inc., Brackenwood Path, Head of the Harbor, St. James, NY 11780

ABSTRACT

We describe methods for measuring dynamical properties for two material categories of interest in understanding large-scale extraterrestrial impacts: iron-nickel and underdense materials (e.g. snow). Particular material properties measured by the present methods include Hugoniot, release paths and constitutive properties (stress vs. strain). The iron-nickel materials lend themselves well to conventional shock and quasi-static experiments. As examples, a suite of experiments is described including six impact tests (wave profile compression/release) over the stress range 2 - 20 GPa, metallography, quasi-static and split Hopkinson pressure bar (SHPB) mechanical testing, and ultrasonic mapping and sound velocity measurements. Temperature sensitivity of the dynamic behavior was measured at high and low strain rates. Among the iron-nickel materials tested, an octahedrite was found to have behavior close to that of Armco iron under shock and quasi-static conditions, while an ataxite exhibited a significantly larger quasi-static yield strength than did the octahedrite or a hexahedrite. The underdense materials pose three primary experimental difficulties. First, the samples are friable; they can melt or sublimate during storage, preparation and testing. Second, they are brittle and crushable; they cannot withstand such treatment as traditional machining or launch in a gun system. Third, with increasing porosity the calculated Hugoniot density becomes rapidly more sensitive to errors in wave time-of-arrival measurements. Carefully chosen simulants eliminate preservation (friability) difficulties, but the other difficulties remain. A family of 36 impact tests was conducted on snow and snow simulants at Sandia, yielding reliable Hugoniot and reshock states, but limited release property information. Other methods for characterizing these materials are discussed.

1. Motivation

The materials properties information required for modeling hypervelocity impacts of asteroids, comets or meteors with other bodies is as follows:

- Hugoniot
- Release properties (continuous release path to zero stress is ideal)
- Material strength information under various strain rate scenarios, varying from quasi-static (strain rate $\leq 10^{-3}$ sec^{-1}) to shock loading (strain rate 10^5 to 10^6 sec^{-1})
- Shock vaporization properties.

Similar information is required for calculating momentum transfer and object breakup in mitigation scenarios.

For materials associated with such hypervelocity impacts, all of these properties except for vaporization may be measured in laboratory settings by such means as impact experiments, split Hopkinson pressure bar (SHPB) measurements and lower strain-rate mechanical testing. Vaporization studies have been undertaken for certain materials [e.g. Wise et al, 1992], but will not be discussed in the present paper.

Three types of materials have been studied in recent Sandia and Los Alamos efforts which are especially pertinent to these problems, specifically recovered meteorite material, underdense materials (natural snow and snow simulants) and silicate rock/mineral compositions representative of bolides.

Iron-nickel compositions such as octahedrite and ataxite represent an important class of asteroids and meteors. We have performed a suite of tests on these materials to determine constitutive response (stress versus strain relation-

*This work was sponsored by the Department of Energy and the Defense Nuclear Agency and conducted at Sandia National Laboratories under the auspices of the Department of Energy under contract DE-AC04-94AL85000.

ships) properties over a wide range of strain rates and over stress ranges to 20 GPa, as well as metallography and ultrasonic property measurements. The results of these tests have contributed to the development of models appropriate for predicting large-scale hypervelocity impact phenomena for iron-nickel materials, or for calculating appropriate methods of deflecting large meteors or asteroids on Earth-intercepting paths.

Underdense materials such as natural snow may represent important constituents of comets. Experimental measurements of dynamic properties of these materials pose three primary difficulties. First, the samples are perishable; they can melt or sublimate during storage, preparation and testing. Second, they are brittle and crushable; they cannot withstand such treatment as traditional machining or launch in a gun system. Third, with increasing porosity the calculated Hugoniot density becomes rapidly more sensitive to errors in wave time-of-arrival measurements. Carefully chosen simulants eliminate preservation (perishability) difficulties, but the other difficulties remain. The results of a family of 36 tests conducted on snow and snow simulants at Sandia will be discussed.

Finally, silicate mineralogies can play an important role in meteor impact situations and mitigation calculations. Methods for measuring appropriate dynamic properties of these materials were discussed in the previous HVIS proceedings [Furnish, 1993a].

There are several experimental constraints of special interest for impact testing of these materials. Sample sizes generally are 4 - 10 mm thick and 6 -7 cm diameter (2 - 2.2 cm diameter for impact velocities of 2.5 - 7 km/sec, where a two-stage light-gas gun must be used). Hugoniot stresses available depend on the exact configuration and material tested. For iron-nickel materials, Hugoniot stresses to 55 GPa may be achieved with the larger diameter samples, and 265 GPa, with the smaller samples. For underdense materials, final stresses are highly sample-dependant. For water ice impacted by tantalum at 2.3 km/sec, for example, a Hugoniot stress of about 10 GPa is produced. With increasing porosity, this stress decreases.

The objective of the present paper is to describe the methods used to acquire these measurements and present representative measurements of iron-nickel and underdense materials.

2. Iron-Nickel Meteorite Material Properties Measurements

To model the impact of an iron-nickel meteorite on a planetary surface or on a spacecraft; or a deflection attempt of an iron-nickel body on an earth-crossing orbit (a Near-Earth Object, or NEO), mechanical properties are required in several regimes. Shock compression and release phenomena dominate material behavior in the immediate vicinity of an impact or strong explosion, with stress levels possibly approaching or exceeding megabar levels over a fraction of the affected volume. At greater distances, lower strain-rate ($\dot{\epsilon}$) processes dominate, for example, governing spall occurring at the antipodal point from such an asteroid.

2.1 Material Descriptions

By contrast with other natural materials such as many rocks, the iron-nickel meteorite materials are macroscopically relatively homogeneous. In other ways as well they are well-suited to dynamic properties measurements: they are durable, non-volatile, and easily and precisely machinable.

Samples of the three common types of metallic meteorites were characterized: Ataxite (Hoba meteorite), Medium-Octahedrite (Henbury meteorite), and Hexahedrite (Coahuila meteorite). Impact testing was performed with material from the Henbury, while all three materials were subjected to constitutive response testing in the Split Hopkinson Pressure Bar and at quasi-static rates.

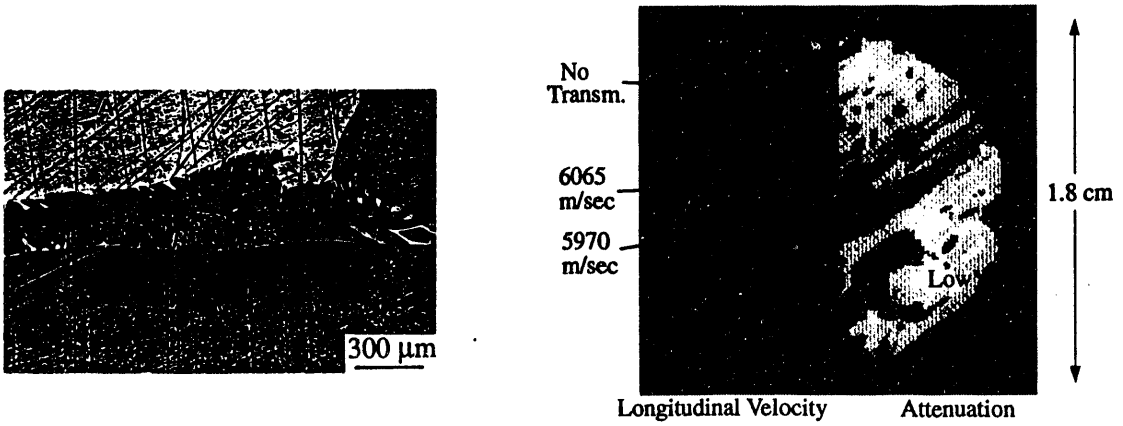

Figure 1. Images of the Henbury material. (Left) Optical metallography, showing deformation twins (labeled "A") in the kamacite. (Right) Representative ultrasonic mapping of sample used for impact tests.

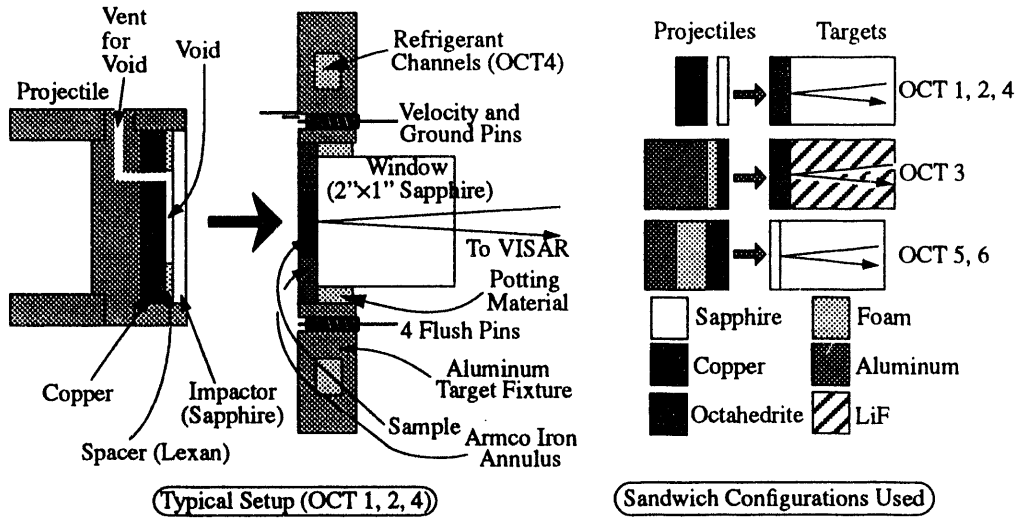

Figure 2. Impact Configurations Used

The Henbury was a central Australian fall, dated about 3,000 BC [Buchwald, 1975]. It has a composition roughly 7.5 wt% Ni, 0.4 wt% Co and 94% Fe (with traces of P, C, S, Cr, Cu, Ge, Ir, Ga and Zn.). The microstructure of the Henbury consists of large lamellar kamacite (bcc-phase; nickel-poor) and mixed regions of taenite and plessite (fcc-phases; nickel-rich) as shown in Figure 1. Numerous deformation twins, labeled "A" in Figure 1, are seen within the kamacite lamellae. This microstructure is consistent with that previously documented as typical in octahedrite meteorites, such as the Henbury [Buchwald, 1975; Remo and Johnson, 1975]. Previous studies have shown the Henbury to consist of ~ 70-80 vol.% kamacite and 20-30% taenite and plessite [Buchwald, 1975], with minor schreibersite ($(Fe,Ni)_3P$) precipitates and occasional troilite nodules.

Ultrasonic studies of the Henbury showed a coarse (2-8 mm) banded, granular structure. This structure is apparent in mappings of the longitudinal velocity and attenuation, with longitudinal velocity variations ranging up to 7% across the samples (Figure 1). Transducer shear velocity measurements made with the particle motion polarized along the bands gave sound velocities averaging 0.85 of the velocities measured for the perpendicular particle velocity motion. Transducer measurements of the longitudinal velocity were also made.

2.2 Impact Experiments

Impact tests performed on the Henbury were designed to allow the observation of strength effects, the Hugoniot, the $\alpha \rightarrow \varepsilon$ transition (in the bcc kamacite component), release properties and whether important effects of a brittle/ductile transition which has been reported at 200K are present. A total of six tests were conducted; configurations used are shown schematically in Fig. 2, with important dimensions given in Table 1.

The wave profiles obtained are shown in Figure 3. These were timed relative to impact according to the ultrasonic longitudinal sound velocity measurements of samples. Those velocities, increased by 15 m/sec, were assumed to equal the elastic (HEL) velocities. Note that experiment OCT-4 utilized a LiF window to allow testing at stresses which would cause sapphire windows to yield. Of particular interest are the elastic precursors (amplitude 0.9 GPa) and the waveform morphology. The waveforms do not suggest an increased brittle component in the 163K test (OCT 4) over the corresponding 300K test (OCT2).

Table 1. Parameters for Impact Tests

Test →	OCT1	OCT2	OCT4	OCT3		OCT5	OCT6
Projectile (thicknesses in mm)							
Cu backer	3.199	3.205	3.189	12.649 (Al)	Al Noseplate	3.199	3.205
Space	0.095	0.254	0.301	4.973 (Foam)	20# Foam	0.095	0.254
Sapphire	3.193	3.193	3.189	1.647 (Cu)	Sample	3.193	3.193
Target (thicknesses in mm)							
Sample	4.999	5.006	4.996	4.999	Sapphire Buffer	4.999	5.006
Window	25.40	25.40	25.40	25.29 (LiF)	Sapphire Window	25.40	25.40
Shot parameters (m/sec)							
Impact Vel.	107	312	311	993		107	312
VPF	40.334	40.608	40.608	55.995		40.334	40.608

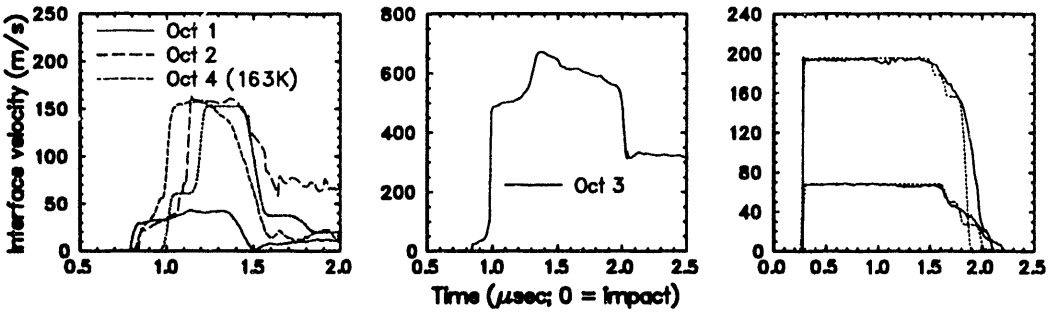

Figure 3. Velocity histories measured for Henbury impact experiments. (Left) Transmitted wave, sapphire window; (center) transmitted wave, lithium fluoride window; (right) reverse-ballistic. Dotted lines are WONDY V modelings assuming Armco iron samples with constant strength of 0.51 GPa.

Two reverse-ballistic (sample in projectile) experiments were conducted to provide a check on Hugoniot measurements as well as further information on release paths. Modeling the two reverse-ballistic waveforms (Figure 3), assuming an elastic-perfectly plastic behavior with no phase transitions, produces good agreement with the observed velocity history. Agreement could be further improved by assuming a more dispersive lower release in OCT 6.

Hugoniot results are summarized in Table 2 for this material. In all cases, the starting density is taken as 7.82 gm/cm^3. For the reverse-ballistic tests (OCT 5 and 6), a precursor of amplitude 0.9 GPa and wavespeed 6 km/sec was assumed. It is interesting that the shock speed for the Hugoniot state in the cryogenic test OCT4 is significantly higher than in the corresponding room temperature test OCT2.

These Hugoniots are plotted against Armco iron data in Figure 4. Lagrangian analysis results and standard P/UP impedance match results are included; only the former are tabulated in Table 2.

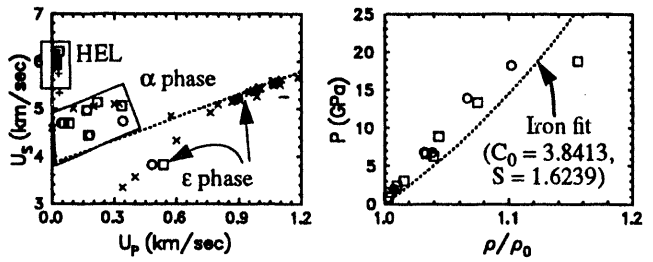

Figure 4. Hugoniot of Henbury Octahedrite. Armco iron Hugoniot for comparison. Impedance match analysis of Hugoniot state in OCT 3 is questionable because of attenuation and difficulty identifying the arrival.
□○ Present Data (Impedance match, Lagrange analysis, resp.)
+ × Armco and other Iron (ρ = 7.85)

The strengths derived from the impact wave profiles ($Y = \sigma_{HEL}\cdot(1-2\nu)/(1-\nu)$; $\nu \equiv$ Poisson's ratio) of 450 MPa are consistent with Hopkinson bar measurements [Furnish, 1994], as well as with Armco iron data [Barker and Hollenbach, 1974].

The α to ε transition was observed in the only impact test above 13 GPa. Its level (13.9 GPa) is similar to that reported for Armco iron (13 GPa [Barker and Hollenbach, 1974]), with a slight elevation probably due to nickel content. The density increase observed here (7%) is similar to that for Armco iron. There is, however, a puzzling post-Hugoniot decay in this waveform which may represent kinetics of the α → ε transition or micromechanical relaxation.

Finally, we do not find evidence in the wave profiles for the ductile - brittle transition inferred for triaxial loading at ~200K [Remo and Anderson, 1975] in the uniaxial shock environment. This is not surprising considering that the present studies probed high rate constitutive response rather than low strain-rate fracture processes. Fracture events depend critically on yield/failure surface interactions which can be stress state dependent and were not considered.

Table 2. Hugoniot states for Henbury octahedrite.

Test #	Particle Vel. km/s	Stress GPa	Density gm/cm^3	Shock Vel. km/s
OCT1	0.043	1.94	7.88	4.69
OCT2	0.182	6.74	8.13	4.44
OCT3	0.481	18.24	8.62	3.82
OCT4	0.167	6.77	8.08	4.97
OCT5	0.078	3.05	7.95	4.69
OCT6	0.218	8.85	8.17	5.13
		α → ε state		
OCT3	0.335	13.93	8.34	5.05
		Elastic precursor states		
OCT1	0.031	1.51	7.862	6.21
OCT2	0.020	0.93	7.849	5.92
OCT3	0.019	0.90	7.848	5.96
OCT4	0.020	0.93	7.849	6.01

2.3 Constitutive properties of NEO materials

Accurate modeling of high energy interactions with NEO (Near-Earth Object) materials requires understanding of the total loading impulse imparted into the object and its effect on material behavior. Following the shock wave produced by the detonation of explosives or by high velocity impact significant inertial dynamic deformation occurs within the loaded material as well as various fracture and fragmentation processes due to multi-wave interactions from non-planar loading and shock release effects. Development of physically-based materials models to contribute to the description of this complex loading history therefore requires an understanding of the influence of the initial shock-loading impulse on the subsequent dynamic deformation and fracture. The dynamic material response driven by inertia from the shock is controlled by how the shock prestraining has altered the material microstructure and its effect on the stress-strain behavior. The dynamic fracture (spallation) behavior of NEO materials is similarly dependent on the starting microstructure, magnitude of the shock prestrain, and duration of the shock process.

Detailed description of the total deformation response of the NEO materials therefore requires: 1) characterization of the starting microstructure of the NEO materials using metallographic and electron microscopic techniques, 2) influence of shock-loading on the structure/property behavior of the NEO materials, 3) influence of strain rate and temperature on the mechanical response of NEO materials, and 4) dynamic fracture (spallation) behavior of NEO materials.

The relationship of stress versus strain for a material (termed the constitutive response) is measured utilizing a variety of experimental techniques. Because mechanical properties such as strength and ductility can vary as a function of temperature, strain rate, and strain, it is necessary to determine these properties under conditions that as closely as possible match the expected deformation rates in service. In the instance of NEO modeling the constitutive data needed encompasses a wide range of strain rates (10^{-3} s^{-1} to shock levels) and temperatures (the cryogenic temperatures representative of deep space versus the rapidly elevated temperatures of high-impulse loading interaction in space, re-entry conditions, or terrestrial impact).

Measurement of the mechanical properties of materials encompasses are very broad field depending on the property of interest, stress-state, temperature, loading rate, environment, etc. and as such will not be reviewed in this paper. Those interested in the diversity and details of mechanical testing should consult Volume 8 of the ASM Metals Handbook [Mechanical Testing, 1985] which covers mechanical testing. For the purposes of providing input to those interested in modeling NEO materials, the constitutive and fracture properties, particularly at high strain rates, are of most immediate concern for use in large scale hydrocode calculations. The constitutive response of metallic and nonmetallic materials, as a function of strain rate and temperature, are most often measured in compression to avoid inertial and wave propagation effects.

Assessment of these properties over a range of strain rates and temperatures comprises the necessary data to benchmark most material models aimed at providing algorithms to quantify the constitutive behavior of materials. Past experience has graphically illustrated the danger of extrapolating these models too far outside the range over which parametric data were measured. At low strain rates, ~ 10^{-4} or 10^{-3} s^{-1} which are termed quasi-static levels, the stress-strain behavior is normally probed using standard screw-driven testing equipment employing right-regular cylindrical samples. Similar sample configurations can also be utilized at strain rates up to nominally 100 s^{-1} strain rates with the addition of hydraulic servo-controlled test machines. With increasing strain rate additional load and strain measurement complexities are imposed. The highest possible strain rates in a uniaxial compression test under uniform deformation conditions is achieved using the Split-Hopkinson Pressure Bar (SHPB). Using this device the constitutive response of metallic samples can be probed over the strain rate range of ~200 to 10^{4} s^{-1}. Combination of the quasi-static testing mentioned previously with SHPB data will allow assessment of the stress-strain response of a material over ~7 orders of magnitude in strain rate. This range represents sufficient data to formulate materials models capable of grasping most of the crucial physics of the deformation response of the material in question with exception of the shock region discussed separately.

Analysis and characterization of the constitutive response of FeNi, chondrite and achondrite meteorite analogs to NEA's will necessarily need to be specific to the type of meteorite to be modeled as there exist substantial differences between metallic types compared to the stonies. Due to the fractured nature of the stonies surviving earth impact, the ability to conduct detailed constitutive studies on these materials representative of NEA materials is significantly impaired, although not lost.

The three metallic meteorite types (hexahedrites, octahedrites, and ataxites) are each based on Fe-Ni alloys with their structural differences arising from the phases formed as dictated by chemical composition. As such the constitutive response of meteorites is not surprisingly linked to that exhibited by their metallic constituents. This can be illustrated by the differences observed in the two predominant metals in metallic meteorites, i e., Iron (Fe) and Nickel (Ni), as a function of strain rate and temperature. The yield stress of body-centered-cubic (BCC) metals, such as Fe and Ta, are markedly temperature dependent, particularly at low temperatures, in contrast to face-centered-cubic (FCC) metals such as Ni or Cu due to this force. Consistent with the observations of polycrystalline unalloyed Fe compared to Ni, decreasing temperature or increasing strain rate is observed to have a drastic affect on the constitu-

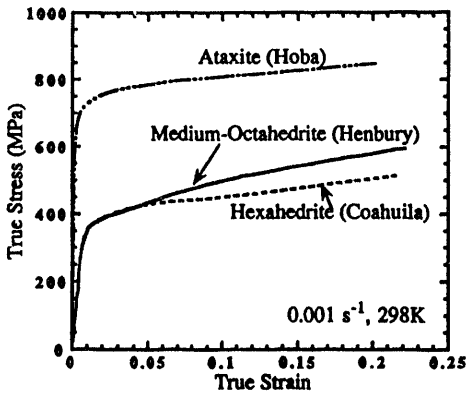

Figure 5: Stress-strain response of 3 metallic meteorite types and the meteorites deformed at quasi-static strain rates and 298K.

tive response of Fe. Both high-rate deformation and testing at cryogenic temperatures are observed to drastically increase the yield strength of Fe. The constitutive response, in particular the yield strength when in an annealed state, of Ni is conversely virtually invariant as a function of strain rate and temperature at low strains. Overcoming the lattice friction stress energy wells in Fe is aided by thermal activation as a dislocation moves from one equilibrium position to the next in the slip plane. Accordingly this stress is dependent on the temperature and strain rate of the deformation. In polycrystalline metals, moving dislocations encounter other dislocations from other slip planes. The stress necessary to pass forest dislocations is dependent on the dislocation density, which in turn is dependent on strain, strain rate, and temperature. Lastly athermal stresses arise from long range barriers to dislocation motion, such as grain or phase boundaries and second phase particles, and can be considered as a fixed value for a given material condition.

Alloys of Fe-Ni, such as in meteorites, depending on whether they are Fe or Ni-rich may exhibit a stress-strain response as a function of temperature and strain rate which lies somewhere between the extremes exhibited by pure Ni or pure Fe or some combination of both depending on the microstructural scale. The addition of non-metallic inclusions or a major volume fraction of a stony component will significantly alter the stress-strain response and our ability to model and predict their response. Assessment of the mechanical properties of meteoritic materials over a range of strain rates and temperatures comprises the necessary data to benchmark any material models aimed at providing algorithms to quantify their constitutive behavior. As an illustration the true stress-true strain response of the three common metallic meteorites; Ataxite-from the Hoba, Medium-Octahedrite from the Henbury, and a Hexahedrite from the Coahuila was measured at as a function of strain rate and temperature. The stress-strain response of the three meteorite types subjected to quasi-static room temperature loading is shown in Figure 5.

The yield strength and work-hardening behavior of all three meteorites are seen to depend on the strain rate and temperature of loading. The quasi-static yield strength of the medium-octahedrite and the hexahedrite are seen to be similar (~350 MPa) while the ataxite is twice as strong (~700 MPa). Compared to their constituents the ~350 MPa yield strength at 0.001 s^{-1} and 298K suggests that both the Henbury and Coahuila are in work-hardened states. The rate of work-hardening for all three meteorites is seen to be reasonably similar. The rate and temperature sensitivity of the yield stress in the Henbury and Coahuila are consistent with: a) the bulk mechanical response of both being controlled by the primary constituent, the bcc kamacite, and b) the work-hardened state of both overall leading to an increased rate and temperature sensitivity compared to annealed pure iron or nickel. While both earth cratering impact and very old events associated with parent break-up can both cause significant shock pulses in meteorites, previous studies suggest it is primarily preatmospheric [Buchwald, 1975]. Cosmic collisions remote in time and space are thought to generate the majority of the substructures and hardening seen in most meteorites [Buchwald, 1975]. The ~factor of two increase in the yield strength in the ataxite is believed to be primarily due to its considerably finer microstructural scale. In-depth metallographic and TEM analysis is underway to elucidate the microstructural aspects controlling the mechanical behavior exhibited by the three different types of metallic meteorites.

The overall differences between meteorite types and the effect of temperature and strain rate on all metallic meteorites illustrates the need for characterizing a range of NEO materials to generate a database from which accurate deformation models and material modeling algorithms can be developed. Accurate models of this type are crucial to the development of physically-based constitutive models to be used in predictive hydrocodes intended for modeling NEO events.

3. Dynamical Properties Measurements of Snow and Other Underdense Materials

3.1 Background

The present study provides data in an important intermediate-stress region for snow and several simulants. Several complementary studies are mentioned for reference. Bakanova et al. [1975] conducted several very-high stress tests

on natural snow of densities of 0.915, 0.60 and 0.35 gm/cm^3, using high-explosive drivers and electrical contact time measurement methods. Maximum stresses measured Hugoniot states up to 50.3, 35.4 and 22.2 GPa (respectively). Johnson et al. [1992a, b] achieved low stresses (to 0.04 GPa) in snow of various densities with an eight-inch gas gun, instrumenting the sample with embedded carbon gauges. They found that (1) the Rankine-Hugoniot jump conditions, although not strictly applicable in this stress region, were not far in error (<10%), and (2) there was little temperature or stress history dependence of the Hugoniot state of the sample. Solie et al. [1994] and Erlich and Curran [1994] were performed contemporaneously with the present study. Solie et al. [1994] detonated sheet explosives at the surface of a snowpack (relatively dry; $\rho_0 \approx 0.25$ gm/cm^3) instrumented with carbon and PVDF gauges. They observed extremely high attenuation. Experimental difficulties included major corrections for the impedance mismatch between the gauges and the snow (giving large error bars for their inferred in-situ states; also a problem for Johnson et al. [1992a,b]) and rapid attenuation (88% in 0.2 m for shock velocity). Adding a sheet to prevent entry of the blast gasses into the snow increased the stress observed at 10 cm by a factor of two. Input stresses ranged to 0.9 GPa. Erlich and Curran [1994] combined yttrium stress gauges and particle velocity gauges to measure the response of artificial snow samples and highly porous grout samples (intended to be of identical material to those used in the present study) to a shock introduced by dilute explosives tiles (DET). Again, rapid attenuation was observed; for example, stresses decreased from 0.1 GPa to 0.025 GPa in 6 cm.

These studies taken together suggest that natural snow gives rapid attenuation where impulsive loading provides stresses of ~0.1 GPa and that the Rankine-Hugoniot wave equations are of restricted value except at very high stress levels or where a nonattenuating wave is indicated.

3.2 Description of technique

Highly distended materials (such as snow and foams) require an experimental geometry somewhat different from those used for iron-nickel, silicate or rock materials, due to the large impedance mismatch existing between the sample and any adjacent components. Consider the configuration shown in Fig. 6.

In most of the present experiments, a thick 6061-T6 aluminum impactor impacts the base of an aluminum (6061-T6) cup containing the sample. A shock is transmitted into the sample. This shock passes through the sample and into a

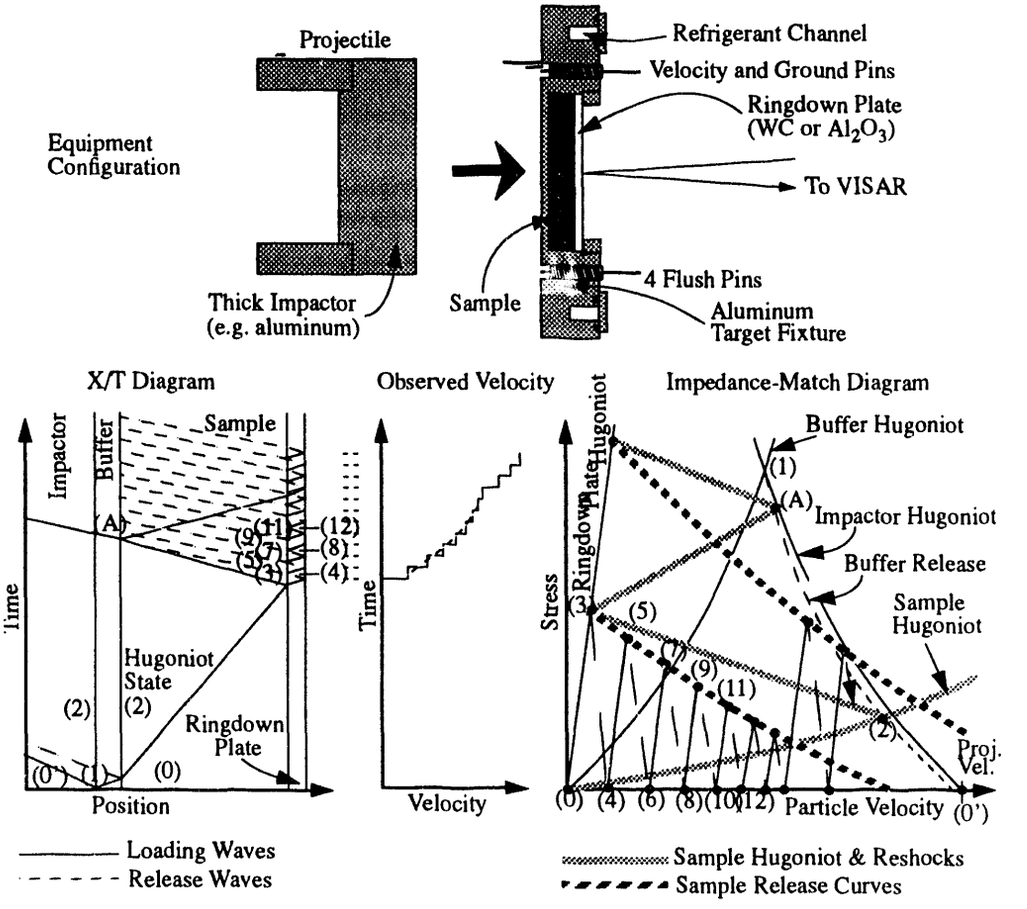

Figure 6. Ringdown Configuration (Gas gun adaptation shown)

thin tungsten carbide plate (the ringdown plate), which is bounded on the other side by a free surface. A reshock passes back into the sample because the tungsten carbide has a higher shock impedance than does the snow or simulant. The plate accelerates downrange (this may also be interpreted as a ringdown). As the plate accelerates, a release wave is sent back into the sample. Velocity interferometry (VISAR) measures the velocity of the free surface of the tungsten carbide plate. Observed free-surface velocities correspond to particle velocities for the states numbered (4+2n) (n = 0, 1, 2, ...) in Fig. 15. Wave profiles are timed relative to impact through the use of a fiducial generated by a flush pin. Corrections applied to this timing include impact planarity, relative travel times of the fiducial and the data from the target to the acquisition instrumentation, and elevation of the flush pin above the impact surface of the target.

It is worth discussing whether the propagating wave can be treated as steady. For experiments conducted with brief impulsive loading, it apparently cannot (see §3.1). The work of Johnson et al. suggested that gas gun results can be interpreted with only minor error as steady-wave. Since the present experiments were conducted at much higher stress levels than were theirs, the error should be yet less important. Therefore, in our analysis, we make the standard assumption that the compression wave is steady.

Equation-of-state information is deduced as follows. Hugoniot states are determined from the shock transit time in the sample, which is calculated from the shock arrival time at the free surface. The Hugoniot state then lies at the intercept of the buffer release curve and the line $\sigma = \rho_0 U_S U_P$. The reshocked stress of the sample is determined from the acceleration of the tungsten carbide plate after the initial ringing has damped. In an experiment with homogeneous samples the velocity increment to the first plateau in the observed velocity history provides the same information, but we have not found such an analysis to be of use with such heterogenous samples as snow, lightweight concretes and grouts. Finally, the stress-volume release trajectory of the sample from the reshock state may be determined from the acceleration history of the free surface according to:

$$\dot{P}_m = P_m \cdot \frac{\sqrt{-\left.\frac{\partial P}{\partial V}\right|_{P_M}}}{\sigma} \quad \text{where} \quad \ddot{x} = \frac{P_m(t)}{\rho_{RP} T_{RP}} \qquad \text{(Eq. 1)}$$

P_m = stress in sample at boundary with ringdown plate
$\rho_{RP} T_{RP}$ = aereal density of ringdown plate
V = specific volume of sample
t = time

The ringdown plate is chosen as a high-impedance material exhibiting a simple wave structure in the stress region of interest. Tungsten carbide (<5% Co binder; density > 14.9 gm/cm^3) may be used at stresses up to about 4.5 GPa (its HEL). This material has a wave velocity of 7.05 km/sec [Steinberg, 1991] . Z-cut sapphire may be used up to about 12 GPa [Graham and Brooks, 1971].

For highly distended materials, the loading wave may be taken as a single wave. Multiwave structures do not normally occur except at extremely low stress levels because the volume change is dominated by porosity collapse.

If cooling is required, liquefied or cold gaseous nitrogen may be passed through the refrigerant channel or acetone chilled by dry ice may be used [Miller and Chhabildas, 1985]. Normally a thermostatic switch is required to avoid large temperature fluctuations. We have used these systems successfully in the ranges of -10°C, -40°C and -90°C [Miller and Chhabildas, 1985] as well as testing natural snow (requiring assembly in a cold room, storage in a freezer and transfer with dry ice in a cooler) [Furnish and Boslough, 1994].

Fractional uncertainties for the Hugoniot density have been shown by Holmes [1991] to be nearly proportional to $(\eta - 1) \equiv (\rho/\rho_0 - 1)$ times the fractional error in shock speed for large compressions. Other important errors are the initial density (which may vary from point to point on the sample) and errors in the release strength of the cup material

This configuration bears close analogies to the ringdown configuration described by Chhabildas and Miller [1985] for measuring the release behavior of crystalline quartz. In their configuration, however, the sample was launched into the ringdown plate. The release measured was from a simple Hugoniot state. Their configuration, however, requires that the sample withstand exposure to vacuum.

3.3 Experimental data and validity assessment

A set of experiments of the above design was performed on natural snow (ρ_0~0.5 gm/cm^3) and two highly porous simulants: (1) A specially formulated lightweight concrete (ρ_0~0.7 gm/cm^3) and (2) a foam cast as interlocked 2 mm spherules coated with Portland cement (r0~0.2 gm/cm3). Waveforms for these experiments are shown in Fig. 7. Hugoniot data extracted from the times-of-arrival are shown with nominal uncertainties in Fig. 8.

Of these 36 tests, 9 were conducted with PVDF stress gauges on both sides of the samples. While these gauges did not give accurate stress levels due to their small size relative to the scale of heterogeneities, they provided additional timing information and indications of reverberations through the sample (e.g. point (A) in Fig. 6).

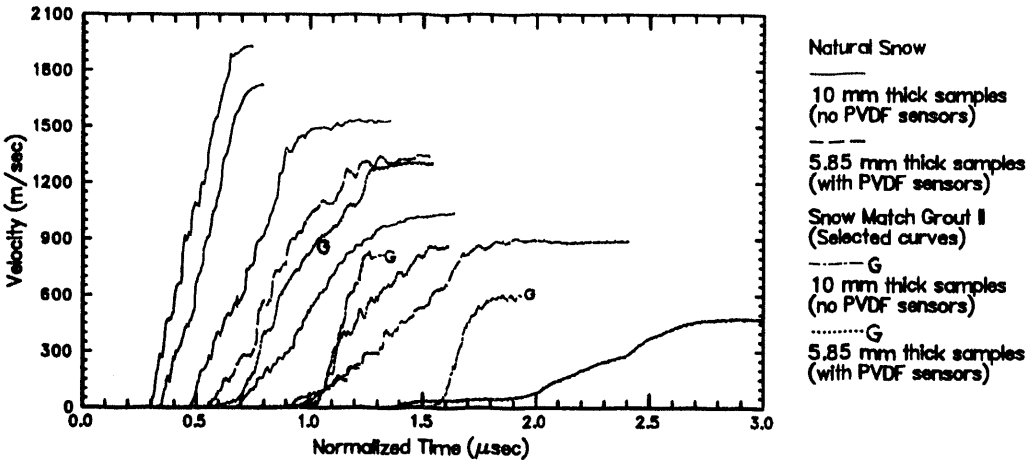

Figure 7. Velocity profiles for natural snow (ρ_0 = 0.5 gm/cm^3), and selected profiles for snow matching grout II (ρ_0 = 0.24 gm/cm^3). Time 0 = shock entering sample. Time normalized for thickness of sample. WC thickness 1.3 mm.

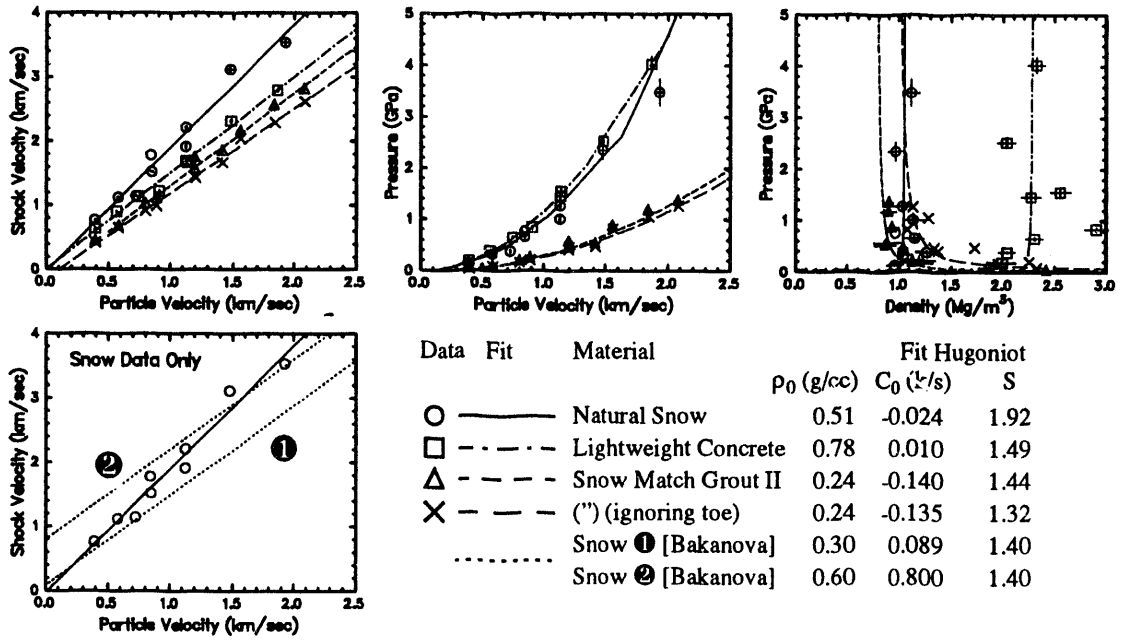

Figure 8. Hugoniot data for snow, distended concrete and foam/Portland cement mixture. Uncertainty bars are shown. Fit curves shown correspond to linear U_S/U_P fits (upper left).

As mentioned earlier, all of the points and fit curves in Figure 8 were derived assuming the initial loading could be described as a steady wave. The unphysical behavior of the Snow-Matching Grout II Hugoniot (see pressure-density space) suggests that for that material this assumption does not hold. This may be related to the "toes" seen for most of the wave profiles for this material, as well as for the lowest-stress snow test (Figure 7). For the distended concrete and the natural snow, however, steady-wave propagation may be a reasonable assumption.

As a demonstration of principal, similar experiments were conducted with Kel-F samples and Bauer-poled PVDF gauges (also using VISAR). Kel-F is a close impedance match to PVDF, so the gauges could be treated to good approximation as part of the sample. These experiments utilized X-cut quartz instead of 6061-T6 aluminum for the impactor and buffer because a sharper shock is produced than if aluminum is used. The wave profile for a representative test is shown in Fig. 9. The reverberation behavior produced in the tungsten carbide is quite well displayed as discrete steps. The period of these steps suggests an average wave velocity of about 6.8 km/sec in the tungsten carbide, slightly lower than the observed small-amplitude velocity of 7.05 km/sec [Steinberg, 1991]. Comparison with a model wave profile calculated with the wavecode WONDY V [Kipp and Lawrence, 1982] shows generally favorable agreement. The machinery discussed above for deducing the Hugoniot, reshock state and release path from the wave profile has been applied, giving the curves shown on the right side of Fig. 9. Perturbations in B0 (an empirical parameter describing part of the release modulus) give an idea of how well the waveform constrains the release path from the reshock state.

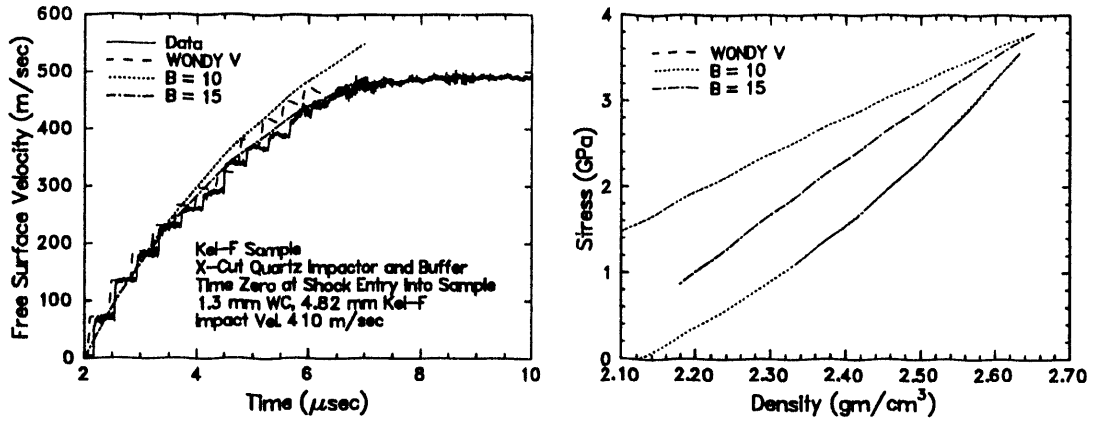

Figure 9. Results of 409 m/sec Kel-F impact experiment. (Left) Ringdown velocity history, with WONDY V modeling and Eq. 1 release modeling superposed. (Right) Corresponding pressure-density curves

Several one-and two-dimensional simulations were performed using the CTH wavecode [McGlaun et al., 1990], with the principal goal of assessing 2-dimensional effects. Experiments chosen from those on snow and the two simulants were simulated. A variety of combinations of zone sizes, material strengths and dimensional assessments were employed. Representative simulations for the 900 m/sec snow impact test are shown in Figure 10. Exactly when two-dimensional effects begin to play a role is slightly ambiguous; the two methods used disagree. Performing a one-dimensional calculation (whether by using an explicitly one-dimensional mesh or a geometry stretched by a factor of ten in the radial direction) gives results which begin to differ from the two-dimensional results as early as 7.3 msec after impact, while comparing the waveforms at the center of the target and 6mm from the center give similar results until 11.3 msec after impact. Two-dimensional modeling discussed in Johnson et al [1992a,b] showed that the arrival of edge effects at the center of an observed interface created an amplified distortion there due to convergence effects. Hence we feels that the comparison of on-axis and displaced velocity histories is the better criterion for estimating when edge effects arrived; i.e. the present data represent uniaxial conditions until about 11 - 11.5 msec after impact.

Several other points should be noted. The Mie-Grüneisen model (based on the Rice-Walsh model of water, with 50% porosity added) gives better overall agreement with the experiment than does the ANEOS model, which was optimized for higher stress levels (and gives a too-stiff Hugoniot state in this situation). Also. the step structure early in the simulated waveforms depends strongly on the choice of zone size, so is interpreted as an artifact of the calculation. Within plausible bounds, variations in strength does not have a strong effect on the wave profile.

4. Concluding Remarks

For iron-nickel materials, high-resolution wave-profile measurements provide Hugoniot, release, constraints on rate dependence, hysteresis. Lower strain rate experiments (SHPB, quasi-static testing) provide complimentary strength and constitutive modeling information. Vaporization studies (not discussed in the present paper) provide important information for energy balancing and blowoff modeling. These data together allow the modeling of a wide range of impact phenomena including meteorite impacts, NEO deflection and asteroid formation.

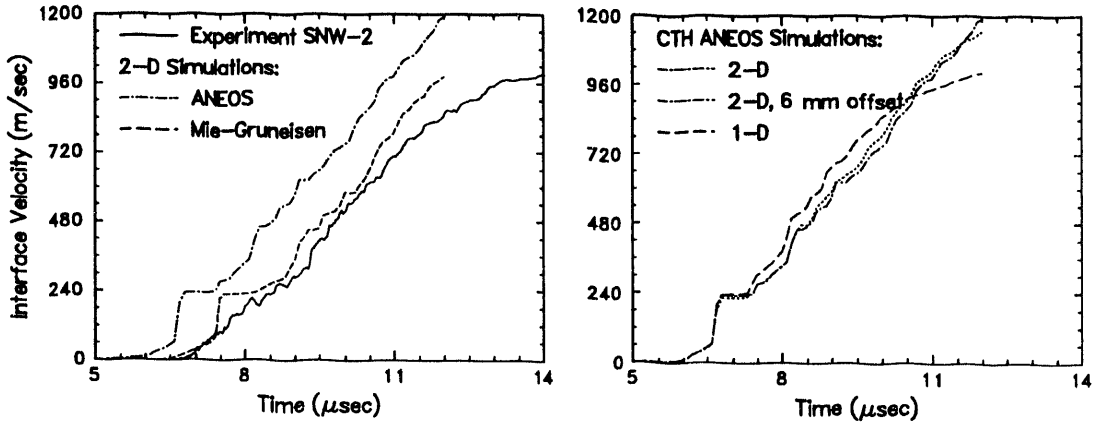

Figure 10. CTH simulations of test SNW-2 (908 m/sec impact velocity). See text for details.

For snow and simulants, it is more difficult to obtain traditional wave profile information due to very low sample impedance, but Hugoniots and reshock levels have been measured, along with limited release information. Complementary attenuation measurements also useful for constraining models; these have been made by other workers. Different applications require different data. For example, calculating airshock coupling into snow requires data for snow containing an ambient air content. On the other hand, calculating a cometary ("dirty snowball") impact on another object may require data for snow containing only a low vapor pressure of water vapor. The knowledge of dynamical vaporization properties required may vary with application as well. Strength issues are important at very low stress levels, but such properties may vary widely in natural snow and ice. Nevertheless, sufficient data are now available to allow a variety of useful calculations of dynamic phenomena for snow and other underdense materials.

5. Acknowledgments

We are grateful to Ron McIntosh and Carl Konrad for handling the myriads of details associated with building up the shots and operating the guns and instruments. Some of the low-density tests and the Kel-F tests were assembled and performed by Dave Wackerbarth and Mike Russell with guidance from Mark U. Anderson. we thank Gary Ganong (RDA) for numerous helpful discussions. Portions of this work were sponsored by the Defense Nuclear Agency (Point of contact: Kent Peterson, SPWE), and other portions by the U. S. Department of Energy, and the entire work was conducted under the auspices of the U. S. Department of Energy under Contract DE-AC04-76DP00789.

References

Bakanova, A. A., V. N. Zubarev, Yu. N. Sutulov and R. F. Trunin, Thermodynamic properties of water at high pressures and temperatures, *Sov. Phys. JETP*, **41**, 544-548, 1975.

Barker, L. M. and R. E. Hollenbach, Laser interferometer for measuring high velocities of any reflecting surface, *J. Appl. Phys*, **43**, 4669-4675, 1972.

Buchwald, V. F., in Handbook of Iron Meteorites, vol. 1, p. 90, U. of Calif. Press, Berkeley, 1975.

Chhabildas, L. C. and J. M. Miller, Release-adiabat measurements in crystalline quartz, Sandia Laboratories Report, SAND85-1092, 1985. See also L. C. Chhabildas and D.E. Grady, Dynamic material response of quartz at high strain rates, *Mat. Res. Soc. Symp. Proc.*, **22** (Pt. III), pp. 147 - 150, 1984. Earlier credit for ringdown technique due to P. C. Lysne, R. R. Boade, C. M. Percival and O. E. Jones, *J. Appl. Phys.*, **40**. 3786, 1969.

Erlich, D. C. and D. C. Curran, An experimental technique for studying shock propagation in large-scale samples of snow and other highly-porous materials, in proceedings of 1993 Joint AIRAPT/APS Topical Group on Shock Compression of Condensed Matter, Colorado Springs, AIP (in press)

Furnish, M. D., Recent advances in methods for measuring the dynamic response of geologic materials to 100 GPa, *Int. J. Impact Engng.*, **14**,, 267-277, 1993a

Furnish, M. D., G.T. Gray III, and J. Remo, Dynamical Behavior of Octahedrite from the Henbury Meteorite, in proceedings of 1993 Joint AIRAPT/APS Topical Group on Shock Compression of Condensed Matter, Colorado Springs, AIP (in press, 1994).

Furnish, M. D. and M. B. Boslough, Impact Studies of the Equation of State of Snow and Snow Simulants, Sandia Report, SAND92-0984 (in preparation).

Graham, R. A. and W. P. Brooks (1971). Shock-wave compression of sapphire from 15 to 420 kbar. The effects of large anisotropic compressions, *J. Phys. Chem Solids*, **32**, 2311-2330.

Holmes, N. C., Equation-of-state measurements of low-density materials, *Rev. Sci. Instr*, **62**, 1990-1994, 1991.

Johnson, J. B., J. A. Brown, E. S. Gaffney, G.L. Blaisdell, and D. J. Solie, Shock response of snow - analysis of experimental methods and constitutive model development, CRREL Report 92-12, 1992a.

Johnson, J. B., J. A. Brown, E. S. Gaffney, G.L. Blaisdell, M. Sturm and S. A. Barrett, Shock wave studies of snow, pp. 107-110 in *Shock Compression of Condensed Matter 1991*, S. C. Schmidt, R. D. Dick, J. W. Forbes and D. G. Tasker (eds)., Elsevier, 1992b.

Kipp, M. E. and R. J. Lawrence, WONDY V - A one-dimensional finite-diference wave propagation code, Sandia National Laboratories report SAND81-0930, 1982.

McGlaun, J. M., S. L. Thompson and M. G. Elrick, CTH- A three-dimensional shock-wave physics code, *Int. J. Impact Engng.*, **10**, 351, 1990

"Mechanical Testing", Volume 8, Metals Handbook-9th Edition, American Society for Metals, Metals Park, Ohio, 1985.

Miller, J. M. and L. C. Chhabildas, A low emperature experimental capability for use with gas guns, Sandia National Laboratories Report, SAND85-0303, 1985.

Remo, J. L. and A.A. Johnson, *J. Geophysical Res.*, **80**, pp. 3744-3748, 1975.

Solie, D. J., J. B. Johnson and S. J. Barret , The response of natural snow to explosive shock waves, in proceedings of 1993 Joint AIRAPT/APS Topical Group on Shock Compression of Condensed Matter, Colorado Springs, AIP (in press)

Steinberg, D. S., Properties of Selected Metals, Lawrence Livermore National Laboratories Report, UCRL-MA-106439, 1991.

Wise,, J. L. G. I. Kerley and T.G. Trucano, Shock-vaporization studies on zinc and porous carbon, pp. 61-64 in *Shock Compression of Condensed Matter 1991*, S. C. Schmidt, R. D. Dick, J. W. Forbes and D. G. Tasker (eds)., Elsevier, 1992.

DATE

FILMED

9/9/94

END